



LAWRENCE
LIVERMORE
NATIONAL
LABORATORY

LLNL-TR-644422

Chlorite Dissolution Kinetics at Variable pH and Temperatures up to 275 °C

S. A. Carroll
M. Smith

September 30, 2013

Chlorite Dissolution Kinetics at Variable pH and Temperatures up to 275 °C

Susan A Carroll & Megan Smith, LLNL

Summary

The objective of this suite of experiments was to develop a useful kinetic dissolution expression for chlorite applicable over an expanded range of solution pH and temperature conditions representative of subsurface conditions in natural and/or engineered geothermal reservoirs. Using our new data and available published data from Smith et al., (2013a) and Lowson et al. (2007), the resulting rate equation is dependent on both pH and temperature and utilizes two specific dissolution mechanisms (an “acid” and a “neutral” mechanism). The form of this rate equation should be easily incorporated into most existing reactive transport codes for to predict rock-water interactions in EGS shear zones.

The dissolution of magnesium-rich chlorite can be described with the following equation and parameters:

$$\text{Rate (mol m}^{-2}\text{s}^{-1}) = \left(\left(k_{\text{acid}} \times e \left[\left(\frac{-E_{\text{acid}}}{R} \right) \times \left(\frac{1}{T} - \frac{1}{298\text{K}} \right) \right] \times a_{\text{H}^+}^n \right) + \left(k_{\text{neut}} \times e \left[\left(\frac{-E_{\text{neut}}}{R} \right) \times \left(\frac{1}{T} - \frac{1}{298\text{K}} \right) \right] \right) \right) (\Delta G_r)$$

normalized to steady-state reactive surface area, where the apparent acid and neutral rate constants at 25 °C are $k_{\text{acid}} = 10^{-9.69}$ and $k_{\text{neut}} = 10^{-12.9}$ ($\text{mol m}^{-2}\text{s}^{-1}$), activation energies for acid and neutral mechanisms are $E_{\text{acid}} = 21.2$ and $E_{\text{neut}} = 20.6$ (kJ mol^{-1}), and the order of reaction with respect to $\text{H}^+_{(\text{aq})}$ is $n = 0.49$.

We find that chlorite dissolution, a sheet-silicate, is relatively slow at these elevated temperatures (100-275 °C), compared to framework silicate minerals for which higher-temperature kinetic data are available (e.g., quartz and feldspars; see Palandri and Kharaka, 2004). This finding is in conflict with previously reported high activation energies for chlorite based on extrapolation of low-temperature experimental data to higher temperatures. Additionally, we note that the dissolution of chlorite does not increase under alkaline conditions, as has been noted for other minerals, but rather remains at the same level minimum value, with only a weak dependence on temperature.

1.0 Introduction

Development of engineered geothermal energy systems (EGS) through the reactivation of fractures in deep hot rocks requires sustained permeability for about 30 years. Chemical reactions pose an important but poorly understood threat to EGS long-term success, because critical kinetic data for fracture minerals at EGS target temperatures necessary to fully assess the risk are lacking. The poor understanding of the impact of rock-water interactions on fracture permeability is illustrated by the variable results from experimental laboratory studies on fractured rock cores. Some data suggest that chemical reactions can significantly reduce fracture permeability even at temperatures much lower than EGS target zones (200 to 400°C) (Polak et al, 2003; Carlson et al, 2005; Viani et al, 2005; Yasuhara et al, 2006, 2011; Yasuhara and Elsworth, 2008), while others in CO₂-rich environments show an increase in fracture permeability (Smith et al., 2013b). It is important correctly assess the role of chemistry on EGS permeability, because reductions in fracture permeability will negatively affect heat transfer, possibly rendering the EGS system uneconomic. In principle the role of geochemistry could be assessed through modeling. Unfortunately, kinetic data and rate equations are lacking for fracture filling minerals at EGS temperatures (200 to 400°C) and are rare even to 100 °C (Cama et al, 2000; Brandt et al., 2003;

Gustaffson & Puidomenech, 2003; Kohler et al., 2003; Carroll and Knauss 2005; Lowson et al., 2005, 2007; Smith et al., 2013a). Use of reaction rates extrapolated from low temperature may over predict dissolution by up to 10,000 times at typical EGS temperatures, leading to poor estimates of impact of geochemical alteration on EGS permeability (Smith et al., 2013a).

We address this need by measuring dissolution rates and deriving rate equations for fracture minerals identified in shear stimulation zones at EGS demonstration sites. The resulting rate equations can be directly incorporated into larger scale reactive transport simulations to assess the impact of geochemical reactions on shear zone permeability. Here we report 20 new chlorite dissolution rates measured from pH 3 to 10 and 100 to 275 °C. These new rate data are combined with previous published data to derive a single rate equation that describes chlorite dissolution from 25 to 275°C from pH 3 to 10 (Lowson et al., 2007; Smith et al., 2013a). We focused on chlorite dissolution kinetics because, chlorite, an Mg- and Fe-bearing sheet silicate, is commonly found in many rock types as both a primary or secondary alteration mineral. This work builds on our previous study of chlorite dissolution for CO₂-EGS applications, by extending the solution pH to capture a wider range of geothermal conditions.

2.0 Materials & Methods

The Mg-rich chlorite used was the same solid as in previous experiments (Smith et al., 2013a) and was purchased from the Source Clays Repository (Purdue, Illinois) as “CCa-2” chlorite, collected from a locality in El Dorado County, California, and described previously by Post and Plummer (1972). The bulk specimen was first crushed to pea-size and then mechanically crushed by micro-milling, with the 150-250 um size fraction collected for use. Approximately 1 g of chlorite was used per experiment. As reported in Smith et al. (2013a), the sample was identified as clinocllore variety, with only trace rutile impurities noted with scanning electron microscopy and electron dispersive spectrometry. Molar mineral dissolution rates reported below were calculated from elemental release data using the stoichiometry determined by Smith et al. (2013a) of $(\text{Mg}_{4.29}\text{Al}_{1.48}\text{Fe}_{0.10})(\text{Al}_{1.22}\text{Si}_{2.78})\text{O}_{10}(\text{OH})_8$. The initial surface area of the unreacted 150-250 um size fraction was measured by multi-point N₂-BET as 4.88 ± 0.30 m²/g, similar to that reported for the hand-crushed samples used in Smith et al. (2013a). Post-reaction sample surface areas were also measured and are reported below. This stoichiometry (specifically the low iron content) and measured surface area differ from those values reported for this mineral by the Clay Minerals Society and has been independently verified by another research group (Black et al., 2013).

All experiments were performed in a background matrix of reagent-grade 0.05m NaCl and distilled deionized water initially purged with N₂ gas to remove atmospheric oxygen. Reagent-grade hydrochloric acid (HCl) and sodium hydroxide (NaOH) were commonly used to adjust the pH of individual solutions to desired levels. Sodium tetraborate (Na₂B₄O₇) was also used as a buffering agent in specific experiments. Total chloride levels in the experimental solutions were maintained at a constant value of 0.05m, but sodium levels varied up to 0.075m as a result of buffers and/or pH adjustment by sodium hydroxide. Experimental solution additions are listed individually in Table 1.

Titanium single-pass mixed-flow reactors (e.g., Dove and Crerar, 1990) were used to conduct chlorite dissolution experiments over a temperature range of 100-275 °C and a pH range of 5-10 at far-from-equilibrium conditions. A schematic of the experimental set-up is shown in Smith et al. (2013a). Room temperature NaCl solutions were pumped into the experimental reactors to pressurize the system, and then the reactor was brought to temperature over a period of several hours while influent solution continued to flow at a constant flowrate of 0.5 mL min⁻¹. We refer to time $t = 0$ in the discussion and figures below as the time when the reactor system achieved its target temperature. Influent

Table 1: Experimental conditions and measured chlorite dissolution rates.

Experiment ID	Temperature °C	Modeled pH at temperature	Si-derived dissolution rate, mol m ⁻² s ⁻¹	Solution pH adjustments
H1A*	100	3.02	1.86 (±0.25) x10 ⁻¹¹	HCl
C18*	100	3.35	7.50 (±0.79) x10 ⁻¹²	[CO _{2(aq)}] = 0.53 mol L ⁻¹
C15*	100	3.49	1.11 (±0.12) x10 ⁻¹¹	[CO _{2(aq)}] = 0.30 mol L ⁻¹
C14*	100	3.57	6.84 (±0.73) x10 ⁻¹²	[CO _{2(aq)}] = 0.20 mol L ⁻¹
C16*	100	3.70	6.60 (±0.69) x10 ⁻¹²	[CO _{2(aq)}] = 0.11 mol L ⁻¹
H1B*	100	4.16	3.19 (±0.34) x10 ⁻¹²	HCl
H1C*	100	5.69	3.74 (±0.40) x10 ⁻¹²	HCl
C21	100	6.01	2.98 (±0.20) x10 ⁻¹²	NaOH
C30	100	6.08	5.86 (±0.57) x10 ⁻¹²	NaOH
C32	100	7.95	4.63 (±0.45) x10 ⁻¹²	Na ₂ B ₄ O ₇ /NaOH
C25	100	9.38	2.56 (±0.24) x10 ⁻¹²	Na ₂ B ₄ O ₇ /NaOH
C11*	150	3.56	1.67 (±0.19) x10 ⁻¹¹	[CO _{2(aq)}] = 0.51 mol L ⁻¹
C8*	150	3.60	1.04 (±0.11) x10 ⁻¹¹	[CO _{2(aq)}] = 0.39 mol L ⁻¹
C19*	150	3.72	2.43 (±0.26) x10 ⁻¹¹	[CO _{2(aq)}] = 0.29 mol L ⁻¹
C13*	150	3.85	3.04 (±0.33) x10 ⁻¹¹	[CO _{2(aq)}] = 0.19 mol L ⁻¹
C12*	150	3.93	1.90 (±0.20) x10 ⁻¹¹	[CO _{2(aq)}] = 0.11 mol L ⁻¹
C20	150	5.59	8.86 (±0.54) x10 ⁻¹²	NaOH
C31	150	5.79	6.69 (±0.65) x10 ⁻¹²	NaOH
C33	150	7.32	5.08 (±0.49) x10 ⁻¹²	Na ₂ B ₄ O ₇ /NaOH
C35	150	9.00	awaiting analysis	NaOH
H2A(repl.)*	200	3.34	1.25 (±0.14) x10 ⁻¹⁰	HCl
H2A*	200	3.63	1.07 (±0.12) x10 ⁻¹⁰	HCl
C7*	200	4.05	4.45 (±0.46) x10 ⁻¹¹	[CO _{2(aq)}] = 0.36 mol L ⁻¹
C10*	200	4.06	9.35 (±1.0) x10 ⁻¹¹	[CO _{2(aq)}] = 0.52 mol L ⁻¹
H2C*	200	4.33	8.07 (±0.87) x10 ⁻¹²	HCl
C6*	200	4.38	8.70 (±0.91) x10 ⁻¹¹	[CO _{2(aq)}] = 0.20 mol L ⁻¹
C9*	200	4.54	7.57 (±0.84) x10 ⁻¹¹	[CO _{2(aq)}] = 0.12 mol L ⁻¹
C9(repl.)*	200	4.54	6.22 (±0.67) x10 ⁻¹¹	[CO _{2(aq)}] = 0.12 mol L ⁻¹
H2B*	200	4.55	5.71 (±0.61) x10 ⁻¹²	HCl
C22	200	5.37	8.20 (±0.53) x10 ⁻¹²	NaOH
C34	200	6.80	7.03 (±0.68) x10 ⁻¹²	Na ₂ B ₄ O ₇ /NaOH
C36	200	7.70	awaiting analysis	NaOH
C27	200	9.00	awaiting analysis	NaOH
C38	250	3.00	awaiting analysis	HCl
C3(repl.)*	250	4.58	4.04 (±0.44) x10 ⁻¹¹	[CO _{2(aq)}] = 0.20 mol L ⁻¹
C3*	250	4.67	3.71 (±0.39) x10 ⁻¹¹	[CO _{2(aq)}] = 0.19 mol L ⁻¹
C5*	250	4.84	2.33 (±0.25) x10 ⁻¹¹	[CO _{2(aq)}] = 0.10 mol L ⁻¹
C23	250	5.51	9.61 (±0.94) x10 ⁻¹²	NaOH
C26	250	7.41	7.25 (±0.60) x10 ⁻¹²	Na ₂ B ₄ O ₇ /NaOH
C37	250	9.00	awaiting analysis	NaOH
H3A*	275	4.41	1.53 (±0.16) x10 ⁻¹⁰	HCl
C1*	275	4.80	2.41 (±0.25) x10 ⁻¹¹	[CO _{2(aq)}] = 0.20 mol L ⁻¹
C2*	275	4.81	2.93 (±0.31) x10 ⁻¹¹	[CO _{2(aq)}] = 0.20 mol L ⁻¹
H3B*	275	5.32	1.64 (±0.17) x10 ⁻¹¹	HCl
H3C*	275	5.40	6.45 (±0.69) x10 ⁻¹²	NaOH
C24	275	5.61	6.86 (±0.66) x10 ⁻¹²	NaHBO ₃ /NaOH
C28	275	7.77	9.12 (±0.87) x10 ⁻¹²	NaOH
C29	275	9.10	awaiting analysis	NaOH

solution was forced to flow upwards past chlorite grains held between fine titanium meshes in an isolated sample holder within the experimental reactor, ensuring continuously mixed conditions of solution-mineral contact. Reactor system pressures were maintained well above boiling point pressures by the use of a dome-loaded back-pressure regulator and nitrogen gas at the reactor outlet. All wetted reactor surfaces (including the pump and back-pressure regulator) were made of C-276 alloy, passivated grade-4 titanium, or PEEK. To conclude each experiment, the reactor heaters were turned off and the sample holder was removed from each reactor as soon as liquid temperatures decreased below 100 °C. Sample holders were dried overnight at 60 °C and chlorite solids were then removed and preserved. Each reactor and pump was cycled with a mildly acidic (pH 4) HCl solution and then at least 24 hours of distilled water rinsing between experiments, and reactor parts were periodically boiled in 8N nitric acid and re-passivated.

Samples were collected directly downstream of the back-pressure regulator through a luer-lock port using 60-mL disposable syringes. Effluent samples were split into three aliquots for analysis: 15 mL were filtered (0.2 µm) and acidified for silicon, magnesium, aluminum, iron, calcium and other trace metal analysis by inductively-coupled plasma mass spectrometry (ICP-MS); 1 mL was filtered and diluted by 10x distilled water for ion chromatography (IC) to confirm consistent background sodium (Na⁺) and chloride (Cl⁻) solution concentrations; 3-5 mL were reserved, unfiltered, for 21 °C pH measurement. The geochemical code EQ3/6 (Wolery, 1992) and the updated *data.shv* database were used to calculate solution pH at experimental temperatures as well as mineral-specific fluid saturation indices. To avoid propagating large errors from IC measurements into the calculation of solution pH, each solution chemistry dataset was first charge-balanced (on chloride, Cl⁻) at 21 °C using measured solution pH values, and then modeled at the experimental temperature for determination of *in situ* solution pH.

3.0 Results & Discussion

In this section we derive chlorite dissolution rate equation from pH 3 – 10 and 25 to 275°C by combining experimental dissolution rates, as determined by silica concentrations measured from new high temperature experiments and previously published experiments (Smith et al., 2013a; Lawson et al., 2007), as well as discuss possible implications of near equilibrium conditions and the observed pH dependence of non-stoichiometric dissolution.

3.1 Derivation of kinetic rate equation

We derived chlorite dissolution rate from pH 3 – 10 and 25 – 275°C by combining experimentally derived dissolution rates from new high temperature experiments and previously published experiments (Smith et al., 2013a; Lawson et al., 2007). As was the case in our past work, the net chlorite dissolution rates were determined from a steady-state change in the measured effluent composition, normalized to flowrate, total surface area and stoichiometric coefficient, as described by equation (1):

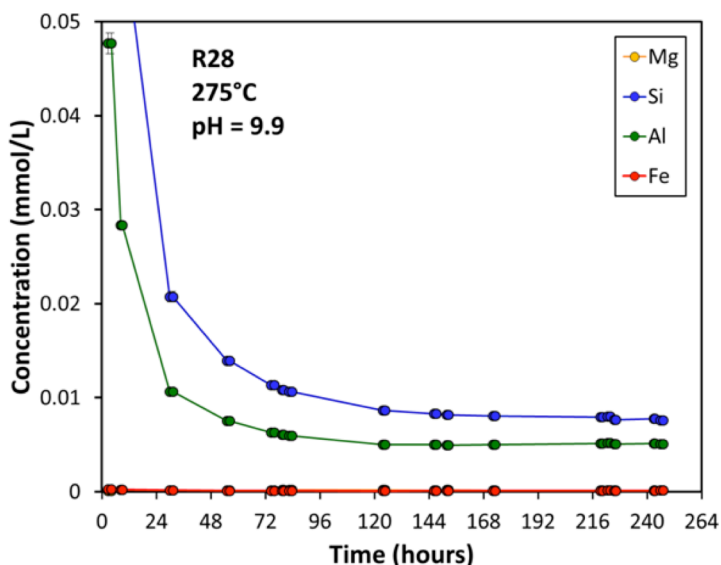


Figure 1: Typical experimental solution chemistry as a function of time for chlorite dissolution experiments conducted with neutral and basic pH solutions.

$$\text{Rate (mol m}^{-2}\text{s}^{-1}) = \left(\left(k_{acid} \times e \left[\left(\frac{-E_{acid}}{R} \right) \times \left(\frac{1}{T} - \frac{1}{298K} \right) \right] \times a_{H^+}^n \right) + \left(k_{neut} \times e \left[\left(\frac{-E_{neut}}{R} \right) \times \left(\frac{1}{T} - \frac{1}{298K} \right) \right] \right) \right) (\Delta G_r) \quad (1)$$

where k represents reaction rate constants (25 °C) for specific rate mechanisms, E represents activation energy values, a_{H^+} is the activity of hydrogen ion, n is an order of reaction term, and R represents the gas constant. Both acid and neutral mechanisms are needed to describe the dependence of chlorite dissolution on pH and temperature. Figure 1 shows an example of the change in silica concentration over time. For experiments conducted at neutral to basic pH, a longer timeframe was necessary to reach steady-state conditions compared to previous experiments performed under more acidic conditions which achieved steady-state levels within 36-72 hours (Smith et al., 2013a).

Figure 2 plots the experimental data and model fit as a function of pH and temperature. At a given temperature, dissolution rates decrease with pH in the acid pH region, achieving a minimum and constant value persisting over neutral to alkaline pH levels. Our observations at high temperature are corroborated by rate versus pH trends observed in lower-temperature (25-95 °C) data published by Lawson et al. (2007). We also intend to include rate data from a third independently collected dataset once published.

In a previous publication, a subset of the data shown in Table 1 (denoted by an asterisk next to the Experimental ID) were used to derive a kinetic dissolution rate equation for acidic conditions (pH<5)

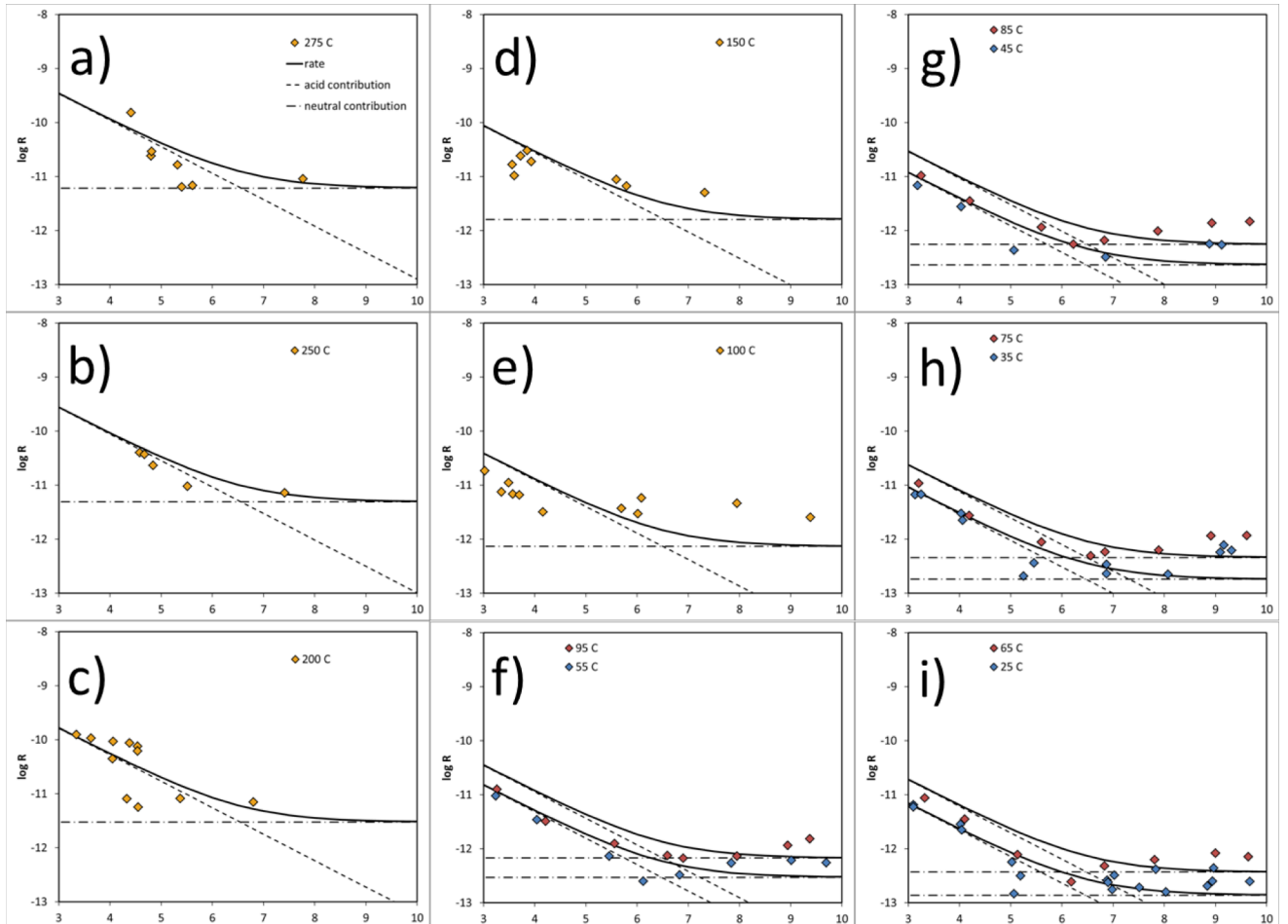


Figure 2: a-i) Log chlorite dissolution rate versus pH at experimental temperatures. Heavy black line represents predicted rate values from the proposed kinetic rate formulation. Fine dashed lines represent individual acid and neutral contributions to the overall dissolution rate. Data from this study (orange) and from Lawson et al. (2007; red and blue).

such as those encountered in a CO₂-Enhanced Geothermal System (CO₂-EGS). Based on that data treatment, which assumed an acid-catalyzed dissolution mechanism, chlorite dissolution was described by three parameters: $n = 0.49$; $E_{acid} = 25.1$ ($kJ\ mol^{-1}$); and $\log k_{acid}$, 25 °C = -9.91 ($mol\ m^{-2}\ s^{-1}$). Inclusion of twenty new data points, collected under neutral and basic solution pH conditions over the same temperature range (100-275 °C) required a second mechanism of dissolution, that was insensitive to pH variations above a certain value ($pH \approx 6$), to fit the data. The data and model fit shown in Figure 2 also include data published by Lawson et al. (2007; see Appendix Table A1) which were collected with a similar single-pass flow-through setup between 25 and 95 °C. Despite a number of differences in the experimental protocol and mineral composition, good agreement was noted at 95 – 100 °C between both studies with similar rate versus pH trends observed at all temperatures.

Optimized model parameters for k_{acid} , E_{acid} , k_{neut} , and E_{neut} (Equation 1) were derived by weighting all data equally and conducting a least-squares linear regression. The value of n was left fixed at 0.49, because it is well constrained by Smith et al. (2013a) and in agreement with other published estimates of this parameter (e.g., Lawson et al., 2005; Brandt et al., 2003; Gustaffson & Puidomenech, 2003). The activation energies, E_{acid} and E_{neut} , were varied first, and then values for 25°C reaction rate constants, k_{acid} , and k_{neut} , were individually varied to optimize the regression coefficient, R^2 . This procedure resulted in optimized values of $E_{acid} = 21.2$ and $E_{neut} = 20.6$ ($kJ\ mol^{-1}$) for the activation energies, which were in agreement with estimates of these values obtained independently through graphical Arrhenius treatment. Reaction rate constant values of $\log k_{acid} = -9.69$ and $\log k_{neut} = -12.9$ ($mol\ m^{-2}\ s^{-1}$). The value for the acid rate constant is similar to that determined previously by Smith et al. (2013a) using the smaller dataset.

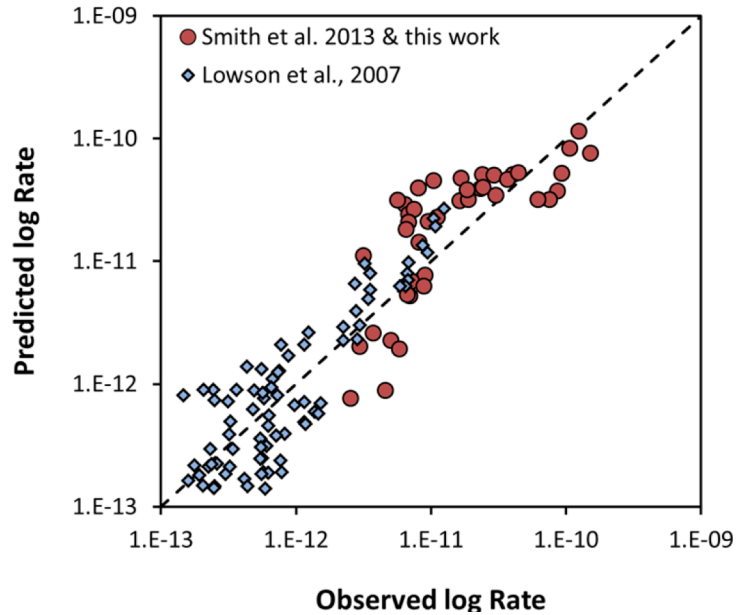


Figure 3: Observed versus predicted chlorite dissolution rates for data from this study Smith et al., 2013a, & Lawson et al. 2007.

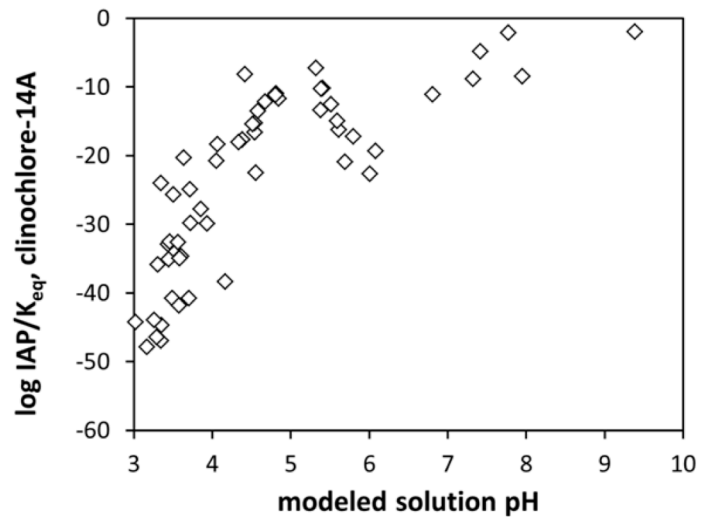


Figure 4: Modeled fluid $\log (IAP/K_{eq})$ values with respect to chlorite (here, variety clinochlore-14A, referenced to data in data.shv database; Wolery, 1992) versus modeled solution pH (at experimental temperature). Data shown here only from this study and Smith et al. (2013a).

A global comparison of the experimental and predicted rates is shown in Figure 3. The overall scatter of the data about the 1:1 (ideal) correlation line is about 0.5 log units, which is comparable to individual errors in the data. It is important to note that over a temperature span of 25-275 °C, the entire dissolution rate dataset only spans a range of 2.5 log units. This rather limited increase in chlorite dissolution rates with temperature suggests that chlorite may not be as reactive as previously thought based on simulations that used rate equations with a much higher temperature dependence (Xu et al., 2005; Wolery and Carroll, 2010).

3.2 Effect of approach to equilibrium on rate magnitudes –

The chlorite rate parameters listed in Section 3.2 assume that the all rate data were measured far from chlorite equilibrium. However, closer inspection of the solution chemistry reveals that this may not be the case for experiments at more alkaline pH values. Figure 4 plots the saturation index (as $\log IAP/K_{eq}$; where IAP = ion activity product and K_{eq} = chlorite equilibrium constant) versus pH for all high temperature data (this work and Smith et al., 2013a). At pH values above ~7, the rates clearly approach chlorite equilibrium. It is important for us to re-evaluate the rate parameters in light of this finding, because the use of rate equations in reactive transport simulations are tied to mineral equilibrium through Gibbs free energy of reaction (ΔG_r) (Equation 1) where

$$\Delta G_r = \left(1 - \frac{IAP}{K_{eq}}\right) \quad (2)$$

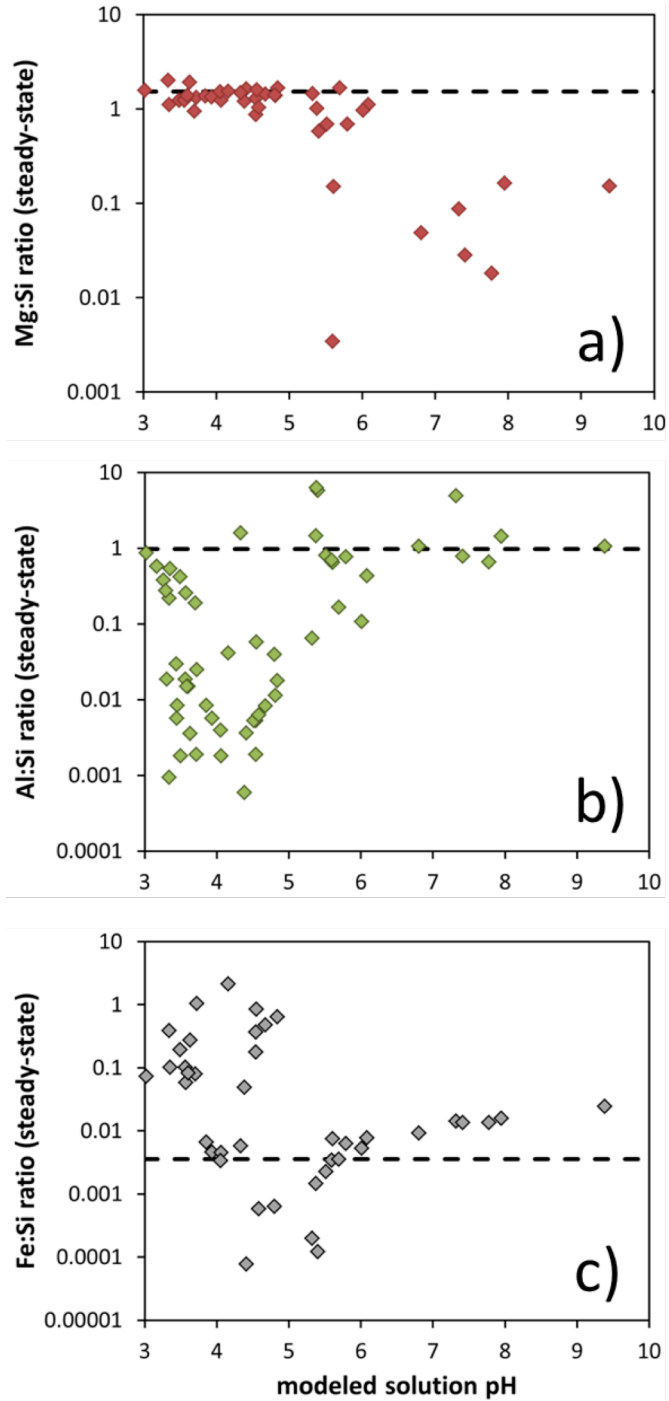


Figure 5: Ratios of steady-state release rates of a) magnesium:silica, b) aluminum:silica, and c) iron:silica versus steady-state modeled solution pH (at the experimental temperature). Dashed horizontal lines represent initial ratios present in unreacted chlorite material.

The Gibbs free energy term allows mineral dissolution to slow as equilibrium is approached, effectively shutting down the chemical reactions. It is possible that some of the scatter observed in fitted data could be attributed to lowering of dissolution rate as equilibrium is approached.

3.3 Stoichiometry of chlorite dissolution – Figure 5 plots the ratios aqueous Mg/Si, Al/Si, and Fe/Si where the dashed lines indicate stoichiometric dissolution as measured by equivalent concentrations in solution and chlorite mineral. Rates reported in Table 1 are derived from Si concentrations rather than Mg or Al (also major constituents of this chlorite variety), because neither magnesium nor aluminum consistently displayed stoichiometric release rates from pH 3 to 9. The trends in Figure 5 suggest possible secondary precipitation of magnesium solids at pH > 6 and of aluminum solids at pH < 6. We will examine the reacted solids using high-resolution transmission electron microscopy (HRTEM) for evidence of the secondary phases. Iron is a minor constituent in the variety of chlorite used in our experiments and shows complex dissolution trends when Fe/Si is plotted against pH. These trends are likely to be an artifact of the experimental set up, because blank (mineral-free) experiments at temperature revealed background iron contributions from the metal reactor and pressure system.

3.4 Changes in reactive surface area – Reacted chlorite grains from neutral and basic solution pH experiments measured in this reporting period displayed surface area values that were about 2 times smaller than the initial unreacted chlorite. Multi-point N₂-BET measurements of different batches of unreacted micro-mill-ground “CCa-2” chlorite grains produced a surface area estimate of 4.9 ±0.3 m² g⁻¹, very similar to the estimate of 5.1 ±0.4 m² g⁻¹ for the hand-crushed “CCa-2” chlorite used in Smith et al. (2013). After reaction for 80-240 hours in solutions of pH ≥5.5, surface area estimates of randomly selected, post-reaction chlorite samples (from experiments C23, C24, and C27) had decreased by approximately 50%, to values of 2.3-2.6 m² g⁻¹. We are currently measuring reacted chlorite samples again and analyzing them with HRTEM to better understand if the change in surface area is real and what it means. One possible explanation for the lower surface areas could be the dissolution of fines grains over the longer experimental durations for the neutral and alkaline experiments. For the purposes of calculating surface-area normalized dissolution rates, we chose to use the post-reaction measured surface area values (2.4 ±0.2 m² g⁻¹), because they are indicative of the conditions during the steady-state periods coinciding with the silica solution chemistry used to derive these rates.

4.0 Conclusions and Implication for EGS

The objective of this suite of experiments was to develop a useful kinetic dissolution expression for chlorite that would be applicable over a wide range of solution pH and temperature conditions representative of subsurface conditions in natural and/or engineering geothermal reservoirs. The resulting rate equation is dependent on both pH and temperature and utilizes two specific dissolution mechanisms (an “acid” and a “neutral” mechanism). Rate parameters were derived from data collected at LLNL and available published data from Lawson et al. (2007). The form of this rate equation (Equation 1) should be easy to incorporate into most existing reactive transport codes for use in prediction of rock-water interactions in EGS systems.

Specifically, we find that the dissolution of chlorite, a sheet-silicate, is relatively slow at elevated temperatures (100-275 °C), compared to other framework silicate minerals for which higher-temperature kinetic data are available (e.g., quartz and feldspars; see Palandri and Kharaka, 2004). This finding is in conflict with previously reported high activation energies for chlorite based on extrapolation of low-temperature experimental data to higher temperatures. Additionally, we note that the dissolution of chlorite does not increase under alkaline conditions, as has been noted for other minerals,

but rather remains at the same level as that noted for neutral conditions, with only a weak dependence on temperature.

Future work includes similar rate measurements and the derivation of useful rate equations for illite, smectite, and biotite from pH 3 to 10 and 100 to 275 °C. Geochemical alteration, changing stress fields, mass transport and heat transfer incorporated into computational models are needed to optimize geothermal energy production for EGS systems. The resulting mineral rate equations from this work can be directly incorporated in modeling efforts to fully assess the impacts of geochemical alteration on long-term fracture permeability for EGS systems across the Geothermal Program.

Chlorite rate equations and data have been submitted to the Geothermal Data Repository.

Acknowledgements

We acknowledge support of this research through the U.S. Department of Energy, Geothermal Technologies Program. We also wish to thank LLNL personnel Victoria Gennetti and Rachel Lindvall (ICP-MS analysis), as well as James Begg and Mavrik Zavarin (N₂-BET analysis). This work was performed under the auspices of the U.S. Department of Energy by Lawrence Livermore National Laboratory under contract DE-AC52-07NA27344. LLNL-TR-644422

References

- Black J, RR Haese. 2013. Chlorite dissolution experiments under CO₂ saturated conditions. Goldschmidt Abstr.
- Brandt F, D Bosbach, R Krawczyk-Bärsch, T Arnold, G Bernhard. 2005. Chlorite dissolution in the acid pH range: A combined microscopic and macroscopic approach. *Geochim et Cosmochim Acta*, 67: 1451-1461. 10.1016/S0016-7037(02)01293-O.
- Cama J., Ganor J., Ayora C., Lasaga C.A. (2000) Smectite dissolution kinetics at 80°C and pH 8.8. *Geochimica et Cosmochimica Acta*, 64, 2701-2717.
- Carlson S.R., Roberts J.J., Detwiler R.L., Viani B.E., Roberts S.K. (2005) Fracture permeability evolution in Desert Peak Quartz Monzonite. *GRC Transactions*, 29, 337-342.
- Dove PM, DA Crerar. 1990. Kinetics of quartz dissolution in electrolyte solutions using a hydrothermal mixed flow reactor. *Geochim et Cosmochim Acta*, 54:955-969. 10.1016/0016-7037(90)90431-J.
- Gustaffson AB, I Puigdomenech. 2003. The effect of pH on chlorite dissolution rates at 25 °C. *Materials Res Soc Symp Proc*, 757:649-655. 10.1557/PROC-757-II3.16
- Köhler S.J., Dufaud F., Oelkers E.H. (2003) An experimental study of illite dissolution kinetics as a function of pH from 1.4 to 12.4 and temperature from 5 to 50°C. *Geochimica et Cosmochimica Acta*, 67, 3583-3594.
- Lowson RT, M-CJ Comarmond, G Rajaratnam, PL Brown. 2005. The kinetics of the dissolution of chlorite as a function of pH and at 25°C. *Geochim et Cosmochim Acta*, 69:1687-1699. 10.1016/j.gca.2004.09.028.
- Lowson RT, PL Brown, M-CJ Comarmond, G Rajaratnam. 2007. The kinetics of chlorite dissolution. *Geochim et Cosmochim Acta*, 71:1431-1447. 10.1016/j.gca.2006.12.008.
- Palandri J, YK Kharaka. 2004. A compilation of rate parameters of water-mineral interaction kinetics for application to geochemical modeling. U.S. Geological Survey Open File Report 2004-1068 (70pp).
- Polak A., Elsworth D., Yasuhara H., Grader A.S., Halleck P.M. (2003) Permeability reduction of a natural reaction under net dissolution by hydrothermal fluids. *Geophysical Research Letters*, 30, 2020, doi:10.1029/2003GL017575.

- Post JL, CC Plummer. 1972. The chlorite series of Flagstaff Hill area, California: A preliminary investigation. *Clays & Clay Min*, 20:271-283.
- Smith MM, TJ Wolery, SA Carroll. 2013a. Kinetics of chlorite dissolution at elevated temperatures and CO₂ conditions. *Chem Geol*, 347:1-8. 10.1016/j.chemgeo.2013.02.017.
- Smith MM, SDC Walsh, WW McNab, Carroll SA. 2013. Experimental investigation of brine-CO₂ flow through a natural fracture: Permeability increases with concurrent dissolution/reprecipitation reactions. Proceedings, 38th Workshop on Geothermal Reservoir Engineering, Stanford University, Stanford, CA (February 11-13, 2013).
- Viani B.E., Roberts J.J., Detwiler R.L., Roberts S.K., Carlson S.R. (2005) Simulating injectate/rock chemical interaction in fracture Desert Peak Quartz Monzonite. *GRC Transactions*, 29, 425-430.
- Wolery TJ. 1992. EQ3/6, a software package for geochemical modeling of aqueous systems. Lawrence Livermore National Laboratory Report UCRL MA-110662-PT-1.
- Wolery TJ, SA Carroll. 2010. CO₂-rock interactions in EGS-CO₂: New Zealand TVZ geothermal systems as a natural analog. *GRC Trans*, 34:729-736.
- Xu T. 2005. Mineral carbonation in a CO₂-EGS geothermal reservoir. Proceedings, 37th Workshop on Geothermal Reservoir Engineering. Stanford University, Stanford, CA (January 30-February 1, 2012).
- Yasuhara H., Polak A., Mitani Y., Grader A.S., Halleck P.M., Elsworth D. (2006) Evolution of fracture permeability through fluid-rock reaction under hydrothermal conditions. *Earth and Planetary Science Letters*, 244, 186-2000.
- Yasuhara H., Kinoshita N, Ohfuji H., Lee D S, Nakashima S, Kishida K (2011) Temporal alteration of fracture permeability in granite under hydrothermal conditions and its interpretation by coupled chemo-mechanical model. *Applied Geochemistry*, 26, 2074-2088.
- Yasuhara H., Elsworth D. (2008) Compaction of a rock fracture moderated by competing roles of stress corrosion and pressure solution. *Pure and Applied Geophysics*, 165, 1289-1306.

Appendix

Table A1: Experimental chlorite dissolution data from Lowson et al. (2007) used in rate equation derivation.

Experiment ID	Temperature °C	Modeled pH at temperature	Log dissolution rate, mol m ⁻² s ⁻¹	Solution pH adjustments
L1	95	3.26	-10.900 ±0.023	KHPhthalate/HCl
L2	95	4.21	-11.490 ±0.016	KHPhthalate
L3	95	5.56	-11.905 ±0.033	H ₃ BO ₃ /HCl
L4	95	6.59	-12.123 ±0.026	KHPhthalate/NaOH
L5	95	6.90	-12.171 ±0.019	K ₂ HPO ₄ /Na ₂ HPO ₄
L6	95	7.95	-12.137 ±0.020	H ₃ BO ₃ /NaOH
L7	95	8.94	-11.936 ±0.020	Na ₂ B ₄ O ₇
L8	95	9.37	-11.814 ±0.026	NaHCO ₃ /Na ₂ CO ₃
L9	85	3.25	-10.978 ±0.015	KHPhthalate/HCl
L10	85	4.20	-11.450 ±0.017	KHPhthalate
L11	85	5.60	-11.937 ±0.018	H ₃ BO ₃ /HCl
L12	85	6.22	-12.252 ±0.019	KHPhthalate/NaOH
L13	85	6.83	-12.180 ±0.019	K ₂ HPO ₄ /Na ₂ HPO ₄
L14	85	7.87	-12.008 ±0.017	H ₃ BO ₃ /NaOH
L15	85	8.93	-11.858 ±0.016	Na ₂ B ₄ O ₇
L16	85	9.67	-11.832 ±0.019	NaHCO ₃ /Na ₂ CO ₃
L17	75	3.20	-10.966 ±0.021	KHPhthalate/HCl
L18	75	4.19	-11.561 ±0.019	KHPhthalate
L19	75	5.60	-12.054 ±0.018	H ₃ BO ₃ /HCl
L20	75	6.56	-12.307 ±0.018	KHPhthalate/NaOH
L21	75	6.84	-12.237 ±0.018	K ₂ HPO ₄ /Na ₂ HPO ₄
L22	75	7.89	-12.201 ±0.018	H ₃ BO ₃ /NaOH
L23	75	8.91	-11.935 ±0.021	Na ₂ B ₄ O ₇
L24	75	9.61	-11.929 ±0.017	NaHCO ₃ /Na ₂ CO ₃
L25	65	3.32	-11.058 ±0.017	KHPhthalate/HCl
L26	65	4.10	-11.450 ±0.019	KHPhthalate
L27	65	5.13	-12.107 ±0.017	H ₃ BO ₃ /HCl
L28	65	6.18	-12.609 ±0.021	KHPhthalate/NaOH
L29	65	6.83	-12.317 ±0.011	K ₂ HPO ₄ /Na ₂ HPO ₄
L30	65	7.81	-12.203 ±0.019	H ₃ BO ₃ /NaOH
L31	65	9.00	-12.081 ±0.018	Na ₂ B ₄ O ₇
L32	65	9.64	-12.146 ±0.018	NaHCO ₃ /Na ₂ CO ₃
L33	55	3.24	-11.022 ±0.016	KHPhthalate/HCl
L34	55	4.04	-11.462 ±0.019	KHPhthalate
L35	55	5.45	-12.133 ±0.025	H ₃ BO ₃ /HCl
L36	55	6.12	-12.599 ±0.024	KHPhthalate/NaOH
L37	55	6.83	-12.483 ±0.023	K ₂ HPO ₄ /Na ₂ HPO ₄
L38	55	7.84	-12.260 ±0.019	H ₃ BO ₃ /NaOH
L39	55	9.01	-12.215 ±0.019	Na ₂ B ₄ O ₇
L40	55	9.69	-12.256 ±0.021	NaHCO ₃ /Na ₂ CO ₃
L41	45	3.18	-11.163 ±0.016	KHPhthalate/HCl
L42	45	4.03	-11.554 ±0.016	KHPhthalate
L43	45	5.06	-12.361 ±0.016	Na ₂ B ₄ O ₇ /HCl
L44	45	6.85	-12.491 ±0.021	K ₂ HPO ₄
L45	45	8.88	-12.247 ±0.016	NaHCO ₃ /HCl
L46	45	9.12	-12.264 ±0.019	Na ₂ B ₄ O ₇ /HCl
L47	45	10.33	-12.115 ±0.029	NaHCO ₃ /Na ₂ CO ₃
L48	35	3.13	-11.173 ±0.019	KHPhthalate/HCl
L49	35	3.25	-11.169 ±0.016	KHPhthalate/HCl

L50	35	4.03	-11.524 ±0.020	KHPthalate
L51	35	4.06	-11.648 ±0.022	KHPthalate
L52	35	5.25	-12.683 ±0.021	H ₃ BO ₃ /HCl
L53	35	5.45	-12.440 ±0.019	H ₃ BO ₃ /HCl
L54	35	6.87	-12.635 ±0.021	K ₂ HPO ₄
L55	35	6.87	-12.467 ±0.023	K ₂ HPO ₄ /Na ₂ HPO ₄
L56	35	8.07	-12.648 ±0.034	H ₃ BO ₃ /NaOH
L57	35	9.09	-12.239 ±0.024	Na ₂ B ₄ O ₇
L58	35	9.16	-12.106 ±0.018	Na ₂ B ₄ O ₇
L59	35	9.31	-12.205 ±0.020	NaHCO ₃ /HCl
L60	35	10.21	-12.519 ±0.026	NaHCO ₃ /Na ₂ CO ₃
L61	35	10.34	-12.251 ±0.018	NaHCO ₃ /Na ₂ CO ₃
L62	25	3.10	-11.186 ±0.022	none noted
L63	25	3.10	-11.225 ±0.017	none noted
L64	25	4.02	-11.545 ±0.031	none noted
L65	25	4.04	-11.649 ±0.020	none noted
L66	25	5.02	-12.244 ±0.017	none noted
L67	25	5.06	-12.830 ±0.018	none noted
L68	25	5.19	-12.501 ±0.023	none noted
L69	25	6.88	-12.582 ±0.022	none noted
L70	25	6.90	-12.622 ±0.018	none noted
L71	25	6.98	-12.752 ±0.019	none noted
L72	25	7.02	-12.490 ±0.017	none noted
L73	25	7.51	-12.716 ±0.019	none noted
L74	25	7.83	-12.378 ±0.019	none noted
L75	25	8.03	-12.797 ±0.019	none noted
L76	25	8.84	-12.689 ±0.020	none noted
L77	25	8.94	-12.601 ±0.019	none noted
L78	25	8.96	-12.358 ±0.022	none noted
L79	25	9.67	-12.605 ±0.021	none noted
L80	25	10.44	-12.226 ±0.023	none noted